Theory of low-threshold optical switching in nonlinear phase-shifted periodic structures

Stojan Radic, Nicholas George, and Govind P. Agrawal

The Institute of Optics, University of Rochester, Rochester, New York 14627

Received June 20, 1994; revised manuscript received October 25, 1994

The theory of phase-shifted nonlinear periodic structures operating in the stationary regime is presented. The transmissive properties of the structure are analyzed by solution of the corresponding set of nonlinear coupled-mode equations exactly. Extremely low switching intensities are found for the special case of $\lambda/4$-shifted structures. An all-optical low-intensity switching configuration that uses a wavelength-tunable source and a $\lambda/4$-shifted nonlinear structure is proposed. Advantages of the phase-shifted distributed-feedback design in all-optical switching applications are discussed.

1. INTRODUCTION

Surprising discoveries concerning optical propagation in nonlinear periodic media[1–5] have renewed interest in nonlinear distributed-feedback (DFB) structures and their use as all-optical switching devices. In recent years these structures and, particularly, their multilayered versions have attracted attention as optical compressors,[6] tunable filters,[7] and bistable devices.[8–10]

Transmission through linear periodic media is characterized by a photonic band structure with stopgaps centered at multiples of the corresponding Bragg frequency. In the presence of material nonlinearity an increase in the field intensity changes the local refractive index, shifting the entire photonics band and making the structure transparent at previously forbidden wavelengths. Even though this picture might be considered a simplified one, it basically explains the mechanism responsible for an all-optical switching process.

It is possible to analyze the operation of a nonlinear uniform DFB device in the stationary (cw) regime and, consequently, to describe its complicated bistable behavior by solving the corresponding set of nonlinear coupled-mode equations exactly.[10] A time-dependent propagation analysis[1,5,11] of the nonlinear periodic structure reveals a rich dynamics that, in special cases, leads to an energy transport in the form of slowly traveling solitary waves, sometimes referred to as the Bragg solitons. Unfortunately, the required switching intensities reported in previous studies are extremely high, varying in the range[10,12] $\sim 0.1-1$ GW/cm^2. Thus, not only are high-power sources needed but thermal problems connected with material absorption at such high intensities introduce additional complications. Coupled with the relatively weak nonlinearities of most optical materials, the above considerations render currently proposed uses of nonlinear DFB structures as a switching device impractical. In recognition of this problem,[9,12–14] much recent effort has focused on optimizing the design of the nonlinear DFB structures by introduction of tapered or segmented periodic structures. Phase-shifted structures can be considered a special case of segmented DFB design. First proposed by Haus and Shank[15] in the form of a $\lambda/4$-shifted structure, phase-shifted gratings are now widely used[16–18] for fabrication of stable single-mode semiconductor laser sources. They can also be used for demultiplexing applications in the case of fiber gratings.[19] A feature of the linear zero-gain $\lambda/4$-shifted configuration is a narrow transmission peak centered in the middle of the Bragg stop band.[18] As the central transmission peak has to be shifted by only a small amount approximately equal to its width, one intuitively expects that switching may occur at input intensities significantly smaller than those necessary for closing the stop band of the uniform DFB structure.

In this paper we present the theory of nonlinear phase-shifted DFB structures operating in the cw regime by solving the corresponding nonlinear coupled-mode equations exactly. As a result, we describe the full input–output characteristics of these devices throughout the entire frequency-tuning region and demonstrate their superiority for low intensity all-optical switching applications. We show that the notion of the central transmissive peak shift is not accurate in the general case and has to be replaced by a more complicated, bistable description that extends in both the intensity- and frequency-tuning domains. Even though we devote most of the our analysis to a $\lambda/4$-shifted device, the theory is valid for arbitrary amounts of the phase shift and can be easily generalized to include multiple phase shifts as well.

The considerable progress made in both use and fabrication of nonlinear, organic materials[20,21] is one of the primary motivations for the present analysis. Kerr-type nonlinearities that are 5 orders of magnitude stronger than those of fused silica have been reported recently.[20] It is not difficult to envisage the first practical ultrafast all-optical switching device built by use of these types of material in combination with optimal low-intensity phase-shifted DFB design. Finally, advances in photosensitive fiber fabrication[21–24] make the writing of periodic patterns directly in the fiber core a feasible and practical procedure, opening yet another possibility for nonlinear DFB fabrication. However, the strength of the silica-fiber nonlinearity is relatively small[25] ($\sim 10^{-16}$ cm^2/W),

0740-3224/95/040671-10$06.00

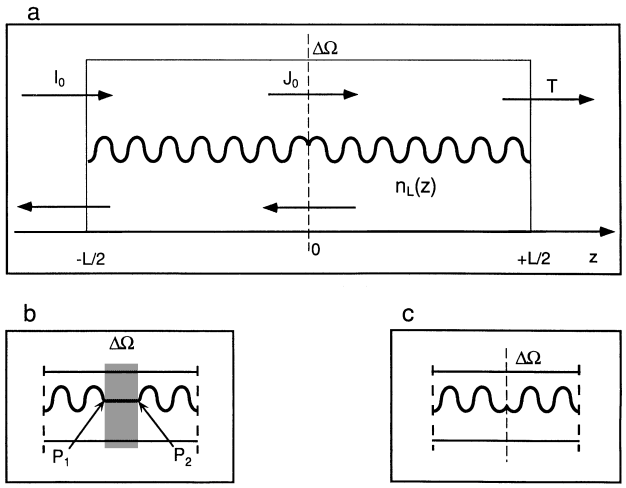

Fig. 1. a, DFB structure with the phase shift $\Delta\Omega$ at the center located at $z = 0$. The sinusoidal curve represents the effective linear index $n_L(z)$. Normalized intensities I_0, J_0, and T are described in text. b, Method of introducing the phase shift by combining two identical periodic regions. The regions are connected by the uniform phase-retarding section that introduces shift of $\Delta\Omega$. c, Phase shift introduced by interrupting the periodicity of a uniform periodic structure. Two segments are regarded as uniform periodic structures differing in phases by $\Delta\Omega$.

a problem that one might address either by extending the length of the periodic structure or by increasing the nonlinearity through fibers made of materials other than silica.

2. NONLINEAR COUPLED-MODE ANALYSIS

A. Formulation of the Problem

Consider the structure shown in Fig. 1a. It has two equal, uniform, periodic regions separated by a phase shift at its center $z = 0$. We refer to these regions as Region 1 ($-L/2 \le z < 0$) and Region 2 ($0 \le z \le L/2$). The desired phase shift can be introduced either by insertion of a uniform slab between the two regions (Fig. 1b) or simply by disruption of the periodicity of the uniform structure at $z = 0$ (Fig. 1c). When the length of the retarder section in Fig. 1b is small compared with the length of each periodic region (i.e., the phase shift is localized), the effect of the two shifting methods on the DFB structure operation is equivalent. Possible realizations in the form of a thin-film waveguide device, a nonlinear multilayer stack, or a fiber grating are not essential to this analysis as long as the standard coupled-mode assumptions can be applied to each case. It is convenient to describe the periodicity of the structure by its linear refractive index:

$$n_L(z) = n_0 + \Delta n \cos(2\beta_B z + \Omega). \tag{1}$$

The Bragg wave vector β_B is given by $\beta_B = 2\pi/\lambda_B$, and the Bragg wavelength λ_B is related to the grating period Λ as $\Lambda = \lambda_B/2n_0$. The constant phase Ω is defined as

$$\Omega = \begin{cases} \Omega_1 & z < 0 \\ \Omega_2 & z \ge 0 \end{cases}. \tag{2}$$

Consequently the phase shift introduced between Region 1 and Region 2 is given by $\Delta\Omega = \Omega_2 - \Omega_1$. The material is assumed to have an instantaneous, isotropic, Kerr-type response described by the nonlinear part of its refractive index, $n_{\mathrm{NL}} \sim {}^1\!/_2 n_2 |E|^2$, where E is the corresponding local electric field. Each uniform region can be modeled by a set of stationary, nonlinear coupled-mode equations,[10,26,27] provided that the standard assumptions of slowly varying envelope and small coupling strength ($\Delta n \ll n_0$) are valid. Following this approach, the electric field throughout the structure is written as the sum of forward- and backward-traveling waves:

$$E(z) = E_+(z)\exp(i\beta z) + E_-(z)\exp(-i\beta z), \tag{3}$$

and the coupled-mode equations that correspond to each region are given by

$$\frac{dE_+}{dz} = i\kappa E_- \exp[-i(2\Delta\beta z - \Omega)] + i\gamma(|E_+|^2 + 2|E_-|^2)E_+, \tag{4a}$$

$$\frac{dE_-}{dz} = -i\kappa E_+ \exp[i(2\Delta\beta z - \Omega)] - i\gamma(2|E_+|^2 + |E_-|^2)E_-. \tag{4b}$$

The parameter $\kappa = \pi\Delta n/\lambda_B$ defines the coupling strength, $\gamma = \pi n_2/\lambda_B$ is the nonlinear parameter governing self- and cross-phase modulation, and $\Delta\beta = \beta - \beta_B$ is the detuning of $\beta = 2\pi/\lambda$ from the Bragg wave vector β_B. We first apply Eqs. (4) to each region independently, without specifying any boundary conditions at the phase-shift position. Region 2 is analyzed first, providing us with field intensity distribution in the region $0 \le z \le L/2$ and, consequently, with the intensity in the center of the structure ($z = 0$). In the second step we impose the proper boundary condition at the interface $z = 0$, connecting the field distributions in Region 1 and 2. We then shift the calculation to Region 1 ($-L/2 \le z < 0$) in order to express the input intensity in terms of the output intensity, which ultimately provides us with the full input–output device characteristics.

Before proceeding to the nonlinear case we briefly discuss the linear DFB structure by setting $\gamma = 0$ in Eqs. (4). The resulting linear equations are easily solved for both uniform and phase-shifted structures.[18] Figure 2 compares the transmittivity as a function of $\Delta\beta$ for the uniform and $\lambda/4$-shifted device by choice of $\kappa L = 4$. The most noteworthy feature is the appearance of the narrow transmission peak for the $\lambda/4$–DFB structure in the center of the Bragg stop band.

B. Uniform Nonlinear DFB Structure

To find the conserved quantities in each region, as given in Appendix A, we separate the magnitude and the phase of the counterpropagating fields as

$$E_\pm(z) = |E_\pm(z)|\exp[i\phi_\pm(z)] = A_\pm(z)\exp[i\phi_\pm(z)], \tag{5}$$

allowing us to calculate the conserved quantities A_T and Γ_i:

$$A_T{}^2 = A_+{}^2 - A_-{}^2, \tag{6}$$

$$\Gamma_i = A_+(z)A_-(z)\cos\psi_i(z) + [2\Delta\beta + 3\gamma A_-{}^2(z)] \times A_+{}^2(z)/(2\kappa), \qquad i = 1, 2. \tag{7}$$

The quantity $A_T{}^2$ can be interpreted as the transmitted flux in each of the regions. It will be shown shortly that

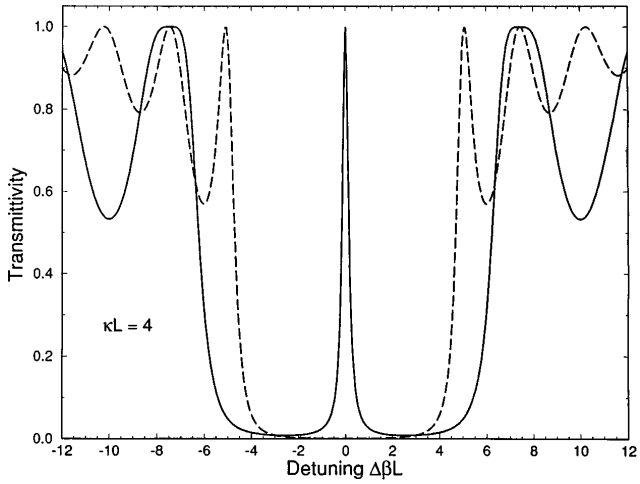

Fig. 2. Transmittivity of linear zero-gain $\lambda/4$-shifted (solid curve) and uniform (dashed curve) DFB structures calculated by the F-matrix method. Both structures are characterized by $\kappa L = 4$.

this quantity remains conserved not only in each region but throughout the entire structure ($-L/2 \le z \le L/2$) as well. The phase ψ_i that appears in Eq. (7) is given by

$$\psi_i(z) = 2\Delta\beta z + \phi_+(z) - \phi_-(z) - \Omega_i\,. \tag{8}$$

We emphasize that Eqs. (6)–(8) describe the quantities A_T and Γ_i, which are conserved in each region independently. Only after we specify the boundary conditions for each interface, and especially those at $z = 0$, can we relate constants in the two regions to each other. In practice, the analysis proceeds from right to left, eventually finding the input intensity I_0 at $z = -L/2$ for a prescribed output T at $z = L/2$. The output intensity plays the role of the initial parameter that is used to express all other field values within the structure. It is therefore natural to impose a boundary condition at the right-hand end ($z = L/2$) of the device first. We assume a nonreflective boundary condition at this interface:

$$A_-(L/2) = 0\,, \tag{9}$$

which immediately defines the forward flux in Region 2 as

$$A_T{}^2 = A_+{}^2(L/2) - A_-{}^2(L/2) = A_+{}^2(L/2)\,. \tag{10}$$

It is of equal importance to recognize that the nonreflecting condition in Eq. (9), together with Eqs. (7) and (10), defines the phase information as well:

$$\begin{aligned}\Gamma_2 &= A_+(z)A_-(z)\cos\,\psi_2(z) + [2\Delta\beta + 3\gamma A^2(z)]A_+{}^2(z)/(2\kappa)\\ &= \Delta\beta A_T{}^2/\kappa\,.\end{aligned} \tag{11}$$

Equation (11), together with Eqs. (A2) and (A3) below, allows us to construct the equation for the forward flux in Region 2:

$$4\kappa^2 A_+{}^2\left[1 - \left(\frac{1}{\kappa A_-}\,\frac{\mathrm{d}A_+}{\mathrm{d}z}\right)^2\right] = A_-{}^2(2\Delta\beta + 3\gamma A_+{}^2)^2\,. \tag{12}$$

In order to normalize intensities, an auxiliary parameter, interpreted as the critical intensity, is introduced as $A_c{}^2 = 8\lambda n_0/3\pi n_2 L$. We perform the normalization by defining the forward flux as $J(z) = [A_+(z)/A_c]^2$, the total transmitted flux as $T = (A_T/A_c)^2$, and the center forward flux as $J_0 = J(0)$. We eliminate the backward flux $A_-{}^2$ by replacing it with $A_+{}^2 - A_T{}^2$. Equation (12) is then reduced to the form

$$\begin{aligned}\left(\frac{L}{2}\,\frac{\mathrm{d}J}{\mathrm{d}z}\right)^2 &= (J - T)[(\kappa L)^2 J - (J - T)(\Delta\beta L + 4J)^2]\\ &= Q(J)\,.\end{aligned} \tag{13}$$

The nonreflective boundary condition at $z = L/2$ that led to construction of Eq. (13) can be replaced by the reflective one in a straightforward manner. We define the reflectance in the form

$$\begin{aligned}r = \frac{E_-(L/2)}{E_+(L/2)} &= \frac{A_-(L/2)}{A_+(L/2)}\,\exp[j(\phi_- - \phi_+)]\\ &= \sqrt{R}\,\exp(-j\theta_R)\,.\end{aligned} \tag{14}$$

From Eq. (8), the phase information at the output is given by

$$\psi_2(z) = \Delta\beta L + \theta_R - \Omega_2\,. \tag{15}$$

The transmitted and the forward fluxes at the device output are related as

$$J\left(\frac{L}{2}\right) = \frac{T}{1 - R}\,. \tag{16}$$

Equations (15) and (16) could now be used to replace Eq. (9) as a starting point of the calculation. However, we proceed by using Eq. (9) because it results in simpler and elegant expressions and discuss the effects of the end reflection in Section 3.B.

The integration of Eq. (13) is the standard elliptical problem whose solution depends on the parameters κL, βL, and T. The polynomial at the right-hand side of Eq. (13) has four zeros that are functions of the above parameters: $J_i = J_i(T, \Delta\beta L, \kappa L)$; $i = 1, 2, 3, 4$. In general, J_i are the complex values that need to be calculated before the integration of Eq. (13) is attempted. In addition, one has to know the relation between limits to be applied in integration of Eq. (13) and the zeros of the polynomial $Q(J)$ as well. For the given transmission intensity T and coupling strength κL, it is possible to distinguish three separate detuning domains in which zeros J_i are either all real or separated into pairs of real and complex conjugate values. To illustrate this, the loci of zeros are plotted in Fig. 3 for fixed values of T ($T = 0.5$) and κL ($\kappa L = 4$). The integration of Eq. (13) is performed within the limits of the center forward flux J_0 and the transmitted flux T:

$$\int_{J_0}^{T} \frac{\mathrm{d}J}{\sqrt{Q(J)}} = \frac{2}{L}\int_0^{L/2} \mathrm{d}z\,. \tag{17}$$

Three detuning domains, defined by the relation between the integration limits and zeros J_i (see Fig. 3), need to be considered separately.

1. *Detuning Domain I in Which* $J_1 \ge J_0 > J_2 = T > J_3 > J_4$

Whereas Fig. 3 clearly shows the relation among the zeros $J_1 > J_2 > J_3 > J_4$, the relation $J_1 \ge J_0 > J_2$ is less obvious. Perhaps the best explanation is given in Ref. 28, in which Eq. (13) is regarded as an energy equation of a classical particle moving in the quartic potential well,

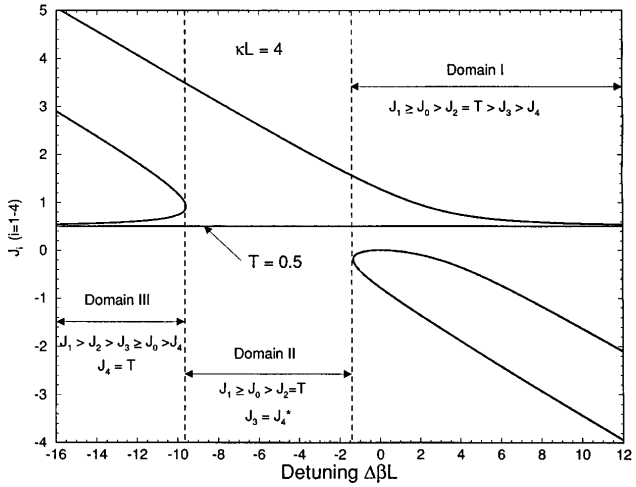

Fig. 3. Loci of the real zeros of the polynomial $Q(J)$ appearing in Eq. (13) for $T = 0.5$ and $\kappa L = 4$. Three detuning domains corresponding to different integration procedures of Eq. (13) are bounded by dashed lines.

$V = -Q(J)$. The zeros J_1 and J_2 then represent the boundaries of the region in which particle ($J_0 \geq 0$) is confined, justifying the relation $J_1 \geq J_0 > J_2$. The integral on the left-hand side of Eq. (17) can be written as[29]

$$\int_{J_0}^{T} \frac{\mathrm{d}J}{\sqrt{Q(J)}} = -\mathrm{sn}^{-1}(\sin\,\phi,\, k)/u\,, \tag{18}$$

where $\mathrm{sn}(\sin\,\phi, k)$ is a Jacobian elliptic function, sine modulus, defined by the argument $\sin\,\phi$ and the modulus k, which are related to the zeros J_i ($i = 1$–4):

$$\sin\,\phi = \left[\frac{(J_1 - J_3)(J_0 - J_2)}{(J_1 - J_2)(J_0 - J_3)}\right]^{1/2}, \tag{19}$$

$$u = 2[(J_1 - J_3)(J_2 - J_4)]^{1/2}\,, \tag{20}$$

$$k = 2[(J_1 - J_2)(J_3 - J_4)]^{1/2}/u\,. \tag{21}$$

Inversion of Eq. (18) gives the center forward flux J_0 in terms of the output flux T:

$$J_0 = J_3 - \frac{J_3 - J_2}{1 - \dfrac{J_1 - J_2}{J_1 - J_3}\,\mathrm{sn}^2(u,\, k)}\,. \tag{22}$$

The dependence $J_0 = J_0(T)$ is here implied through $J_i = J_i(T)$. In the case of zero detuning ($\Delta\beta L = 0$), the zeros of the polynomial $Q(J)$ take a particularly simple form,[10] allowing us to simplify Eq. (21) by means of Landen's transform[29]:

$$J_0 = T[1 + \mathrm{nd}(\kappa L x,\, 1/x)]/2\,. \tag{23}$$

The parameter x used in inverse amplitude function nd is given by $x = [(2T/\kappa L)^2 + 1]^{1/2}$. In further calculations, when the expression for zero-detuning flux J_0 is needed, we use the compact form of Eq. (23) rather than Eq. (22).

2. Detuning Domain II in Which
$J_1 \geq J_0 > J_2 = T$, $J_4 = J_3{}^*$
The left-hand integral in Eq. (18) is now solved as[29]

$$\int_{J_0}^{T} \frac{\mathrm{d}J}{\sqrt{Q(J)}} = -\mathrm{cn}^{-1}(\cos\,\phi,\, k)/u\,, \tag{24}$$

where cn is a Jacobian elliptic function, cosine modulus, defined by its argument and modulus:

$$\cos\,\phi = \frac{(J_1 - J_0)B - (J_0 - J_2)A}{(J_1 - J_0)B + (J_0 - J_2)A}\,, \tag{25}$$

$$u = 4\sqrt{AB}\,, \tag{26}$$

$$k^2 = [(J_1 - J_2)^2 - (A - B)^2]/(4AB)\,. \tag{27}$$

The parameters A and B are defined as $A = |J_1 - J_3|$ and $B = |J_2 - J_3|$, respectively. Inversion of Eq. (24), together with Eq. (17), enables us to calculate the center forward flux J_0 in this detuning region in the following form:

$$J_0 = J_2 + \frac{J_1 - J_2}{1 + \dfrac{|J_1 - J_3|}{|J_2 - J_3|}\,\dfrac{1 + \mathrm{cn}(u,\, k)}{1 - \mathrm{cn}(u,\, k)}}\,. \tag{28}$$

3. Detuning Domain III in Which
$J_1 > J_2 > J_3 \geq J_0 > J_4 = T$
In detuning domain III Eq. (19) takes the form[29]

$$\sin\,\phi = \left[\frac{(J_1 - J_3)(J_0 - J_4)}{(J_3 - J_4)(J_1 - J_0)}\right]^{1/2}. \tag{29}$$

The modulus k and the argument u are unchanged and are given by Eqs. (17) and (18). In this detuning domain the center forward flux is found to be

$$J_0 = J_1 - \frac{J_1 - J_4}{1 - \dfrac{J_3 - J_4}{J_3 - J_1}\,\mathrm{sn}^2(u,\, k)}\,. \tag{30}$$

We can now use Eqs. (19)–(30) to illustrate the change in the transmissive behavior of the uniform DFB structure with the increasing field intensity. The switching process can be understood as one that closes the Bragg stop band as the field intensity is increased. This is clearly evident in Fig. 4, where the transmission of a uniform DFB structure is plotted for increasing values of output field intensities T.

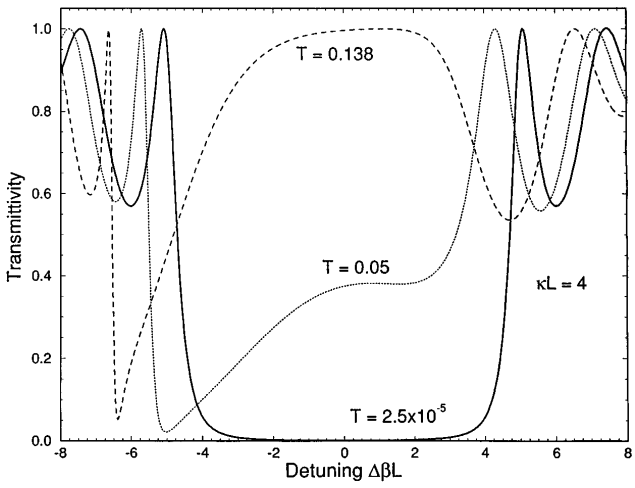

Fig. 4. Transmittivity of the nonlinear, uniform DFB structure for three values of the normalized output T and $\kappa L = 4$. The solid curve corresponds to the case $T = 2.5 \times 10^{-5}$, the dotted curve represents $T = 0.05$, and the dashed curve represents $T = 0.138$.

C. Phase-Shifted Nonlinear DFB Structure

The knowledge of the center forward flux J_0, together with the phase information given by Eq. (11), defines the electric field at the interface $z = 0$. In order to proceed with the analysis, we have to relate J_0 and phase information from Region 2 to the field intensity and phase in Region 1. The role of the structure's central region is to introduce a phase shift $\Delta\Omega$ between the counterpropagating waves as they cross from one region to another. In case of the phase-shifting method shown in Fig. 3b the forward- and backward-traveling field components acquire the desired phase shift of $\Delta\Omega$ by passing the distance $\overline{P_1P_2}$. Each region is assumed to have an equal number of grating periods and a constant grating phase Ω_i. The phases of the adjacent regions are related by $\Omega_2 = \Omega_1 + 2\pi m$, where m is an integer. For the phase-shifting method shown in Fig. 3c, however, grating phases Ω_1 and Ω_2 differ by $\Delta\Omega$, while the counterpropagating fields remain continuous at $z = 0$. Even though the end effect of both methods on the transmission characteristics is the same, we find it more convenient to proceed by using the latter method (Fig. 3c) and the continuity condition associated with it:

$$E_{\pm}(0-) = E_{\pm}(0+). \tag{31}$$

A shorthand notation $\lim_{\epsilon\to 0} E_{\pm}(0 \pm \epsilon) = E_{\pm}(0\pm)$ has been used in Eq. (31).

Continuity condition (31) together with Eq. (6) leads to a simple expression for the transmitted flux throughout the entire structure ($-L/2 \le z \le L/2$):

$$A_{T1}{}^2 = A_+{}^2(0-) - A_-{}^2(0-) = A_{T2}{}^2 = A_+{}^2(0+) - A_-{}^2(0+) = A_T{}^2. \tag{32}$$

Equation (32) shows that the transmitted flux remains a conserved quantity throughout the entire nonuniform structure. This can be regarded as the special case of the Poynting law applied to our phase-shifted device. We obtain the phase information in Region 1 by applying Eq. (7) to Region 1:

$$\Gamma_1 = A_+(0)A_-(0)\cos\,\psi_1(0) + [2\Delta\beta + 3\gamma A^2(0)]A_+{}^2(0)/(2\kappa). \tag{33}$$

The counterpropagating magnitudes $A_{\pm}(0)$ are to be expressed through the center forward and transmitted fluxes, J_0 and T. Also, we have to relate the phase $\psi_1(0)$ to known or calculated parameters in Region 2 in order to construct an equation for the forward flux in Region 1 similar to Eq. (12). Once this equation is written, the field intensity in this region ($-L/2 \le z < 0$), and the input intensity I_0 at $z = -L/2$, can be calculated in terms of T. From Eqs. (8) and (31) it follows that

$$\psi_1(0) = \psi_2(0) - \Delta\Omega. \tag{34}$$

Equation (34) effectively closes the problem: for a given phase shift $\Delta\Omega$ and $\cos\,\psi_2(0)$ calculated in Region 2 it is always possible to find Γ_1 and, therefore, to construct the equation for forward flux in Region 1. In this special case when $\Delta\Omega = \pi$ ($\lambda/4$-shifted device), Eqs. (33) and (34) can be combined to give the following expression for Γ_1:

$$\Gamma_1 = -A_c{}^2 J_0\sqrt{J_0 - T}\,\cos\,\psi_2(0) + [2\Delta\beta + 3\gamma A_c{}^2(J_0 - T)]A_c{}^2 J_0/(2\kappa). \tag{35}$$

We eliminate the field magnitudes A_+ and A_- in Eq. (35) by replacing them with $A_c\sqrt{J_0}$ and $A_c\sqrt{J_0 - T}$, respectively. To eliminate $\cos\,\psi_2(0)$ from the last relation we apply Eq. (11) for the case of $z = 0$:

$$A_+(0)A_-(0)\cos\,\psi_2(0) + [2\Delta\beta + 3\gamma A_-{}^2(0)]A_+{}^2(0)/(2\kappa) = \Delta\beta A_T{}^2/\kappa.$$

Elimination of $A_{\pm}$ gives the final form for $\cos\,\psi_2(0)$:

$$\cos\,\psi_2(0) = -\frac{1}{\kappa L}\left(\frac{J_0 - T}{J_0}\right)^{1/2}(4J_0 + \Delta\beta L). \tag{36}$$

Use of Eq. (36) in Eq. (35) defines the conserved quantity Γ_1 in Region 1:

$$\Gamma_1 = [8J_0(J_0 - T) + (\Delta\beta L)(2J_0 - T)]A_c{}^2/(\kappa L). \tag{37}$$

The procedure that led to the forward flux equation in Region 2 can now be replicated in Region 1. For any point in Region 1, combination of Eqs. (7) and A(2) and A(3) below leads to

$$4\kappa^2 A_-{}^2 A_+{}^2\left[1 - \left(\frac{1}{\kappa A_-}\,\frac{\mathrm{d}A_+}{\mathrm{d}z}\right)^2\right] = [2\kappa\Gamma_1 - (2\Delta\beta + 3\gamma A_-{}^2)^2 A_+{}^2]^2. \tag{38}$$

Again, we normalize Eq. (38) by introducing the intensities: $I = A_+{}^2(z)/A_c{}^2$ and $I_0 = I(0)$. Elimination of Γ_1 from Eq. (38) gives the final equation for the forward flux in Region 1:

$$\left(\frac{L}{2}\,\frac{\mathrm{d}I}{\mathrm{d}z}\right)^2 = (\kappa L)^2 I(I - T) - [8J_0(J_0 - T) - 4I(I - T)]^2 = P(I). \tag{39}$$

It is interesting to compare the forms of Eqs. (13) and (39). They correspond to an identical class of elliptic problems, differing only in position of the zeros of the corresponding right-hand polynomials. As an illustration, the loci of real zeros of the polynomial $P(I)$ from Eq. (39) are plotted in Fig. 5 for a fixed value of the transmitted flux $T = 0.1$ and a coupling strength of $\kappa L = 4$. We plot the center forward flux J_0 as a dashed curve in order to show its relation to zeros I_i of $P(I)$ throughout the detuning region. Once again, three detuning domains are clearly resolved. As the intradevice intensity increases, the domain positions are shifted toward lower frequencies, while the allowed regions are widened at the same time. Finding the zeros I_i of the polynomial on the right-hand side of Eq. (39) requires solving the general quartic equation $P(I) = 0$. Because the analytic solution of this equation in the general case proves to be quite an involved procedure, the zeros I_i are usually found numerically. In the special case of zero detuning ($\Delta\beta L = 0$), these zeros can be written in a relatively simple form:

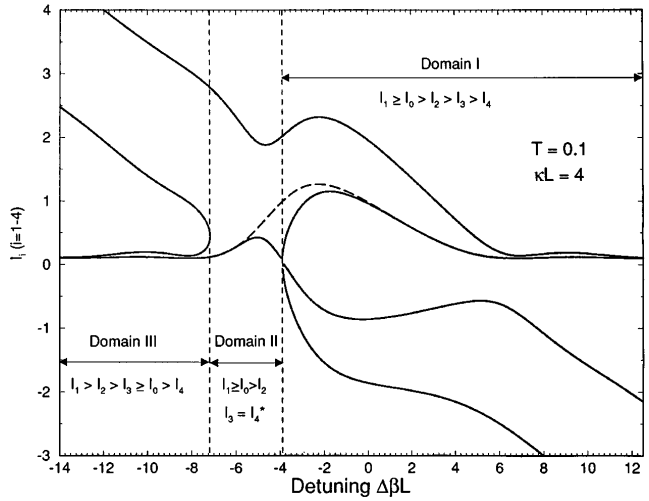

Fig. 5. Loci of the real zeros of the polynomial $P(I)$ that appears in Eq. (39) for $T = 0.1$ and $\kappa L = 4$. The dashed curve represents the center-forward flux J_0 and its relation to the zeros of the $P(I)$. Three detuning domains indicate regions in which different solutions of Eq. (39) are valid.

$$I_i = \frac{T}{2}\left\{1 \pm \frac{k}{k'}\left[\eta \pm \sqrt{\eta + k^2}\right]^{1/2}\right\}, \qquad i = 1, 2, 3, 4. \quad (40)$$

The parameter η is defined here as $\eta = k'^2[2(\mathrm{nd}^2(u, k) - 1) + k^2]/k^2$. Function $\mathrm{nd}(u, k)$ is given by Eq. (23), and $k' = \sqrt{1 - k^2}$ is the complement of the modulus k.

The integration of Eq. (39) is performed within the limits I_0 and J_0 such that

$$\int_{I_0}^{J_0} \frac{\mathrm{d}I}{\sqrt{P(I)}} = \frac{2}{L}\int_{-L/2}^{0} \mathrm{d}z\,. \quad (41)$$

The integral on the left-hand side of Eq. (41) can be separated in the form

$$\int_{I_0}^{J_0} \frac{\mathrm{d}I}{\sqrt{P(I)}} = \int_{I_0}^{I_2} \frac{\mathrm{d}I}{\sqrt{P(I)}} + \int_{I_2}^{J_0} \frac{\mathrm{d}I}{\sqrt{P(I)}} = \int_{I_0}^{I_2} \frac{\mathrm{d}I}{\sqrt{P(I)}} + F(\phi, k)/u\,. \quad (42)$$

The second integral on the right-hand side of Eq. (42) is easily evaluated as the incomplete elliptic integral of the first kind, provided that the center forward flux J_0 is known. Arguments ϕ and u and modulus k will be defined for each detuning domain in which the integration of Eq. (41) is performed. Combining Eqs. (41) and (42), we can write the integral equation for the input intensity I_0:

$$\int_{I_2}^{I_0} \frac{\mathrm{d}I}{\sqrt{P(I)}} = F\{\phi[J_0(T)], k(T)\}/u(T) - 1\,. \quad (43)$$

By indicating dependencies $u = u(T)$, $\phi = \phi[J_0(T)]$, and $k = k(T)$ we emphasize the relation $I_0 = I_0(T)$ between the input and output fluxes. As in the case of Eq. (17), which has been used to calculate center forward flux J_0, it is necessary to invert Eq. (41) and calculate input intensity I_0 in terms of the output intensity T. Using the formulas given in Eqs. (19)–(30), one can easily calculate I_0 for each detuning domain.

1. Domain I in Which $I_1 \geq I_0 > I_2 > I_3 > I_4$ and $I_1 \geq J_0 > I_2 > I_3 > I_4$

It is not necessary to know the relation between I_0 and T in order to calculate I_0. Input intensity in this domain is given by Eq. (22) with the substitution $J_i \rightarrow I_i$:

$$I_0 = I_3 - \frac{I_3 - I_2}{1 - \dfrac{I_1 - I_2}{I_1 - I_3}\,\mathrm{sn}^2(v, k)}\,. \quad (44)$$

Argument v is given by $v = F(\phi, k) - u$, and ϕ, u, and k are given by Eqs. (19)–(21) and the substitution $J_i \rightarrow I_i$, $i = 1, 2, 3, 4$.

2. Domain II in Which $I_1 \geq I_0 > I_2$ and $I_1 \geq J_0 > I_2$, I_3 and $I_4 = I_3^*$

Input intensity is calculated by Eq. (28) and the substitution $J_i \rightarrow I_i$:

$$I_0 = I_2 + \frac{I_1 - I_2}{1 + \dfrac{|I_1 - I_3|}{|I_2 - I_3|}\,\dfrac{1 + \mathrm{cn}(v, k)}{1 - \mathrm{cn}(v, k)}}\,. \quad (45)$$

Argument v is given by $v = F(\phi, k) - u$, and ϕ, u, and k are given by Eqs. (25)–(27) and the substitution $J_i \rightarrow I_i$; $i = 1, 2, 3, 4$.

3. Domain III in Which $I_1 > I_2 > I_3 \geq I_0 > I_4$ and $I_1 > I_2 > I_3 \geq J_0 > I_4$

In domain III the limit I_2 in the right-hand integrals of Eq. (42) has to be replaced by I_4. The input intensity I_0 is given by Eq. (30) and the substitution $J_i \rightarrow I_i$:

$$I_0 = I_1 - \frac{I_1 - I_4}{1 - \dfrac{I_3 - I_4}{I_3 - I_1}\,\mathrm{sn}^2(v, k)}\,. \quad (46)$$

Argument v is given by $v = F(\phi, k) - u$, and ϕ, u, and k are given by Eqs. (20), (21), and (29) and the substitution $J_i \rightarrow I_i$; $i = 1, 2, 3, 4$.

The inversion of the elliptic function sn by means of $F(\phi, k)$ requires the knowledge of phase ϕ, even though $\sin\phi$ or $\cos\phi$ is known [Eqs. (19), (25), and (29)]. The functions $\sin^{-1}\phi$ and $\cos^{-1}\phi$ are multivalued, raising the possibility of choosing the improper solution branch. We verify the consistency of the solutions in two regions by checking the continuity of the flux axial derivative at $z = 0$ for the case of $\Delta\Omega = 0$ (uniform device). Only one solution branch will satisfy the continuity of the field derivative at the center of the device, thus uniquely defining the solution in the first region.

3. DISCUSSION AND NUMERICAL RESULTS

A. Zero-Detuning Transmission

To illustrate the salient features of the preceding analysis, we consider the zero-detuning case first ($\Delta\beta L = 0$) by applying Eqs. (40) and (44). As a consequence of the central transmission peak shift (see Fig. 2), the efficiency of the structure is expected to fall off rapidly as the input intensity is increased. Figure 6 shows the transmittivity as a function of the normalized input intensity I_0 for coupling strengths varied from $\kappa L = 3$ to $\kappa L = 6$. For a moderate coupling strength ($\kappa L = 6$), it is necessary only

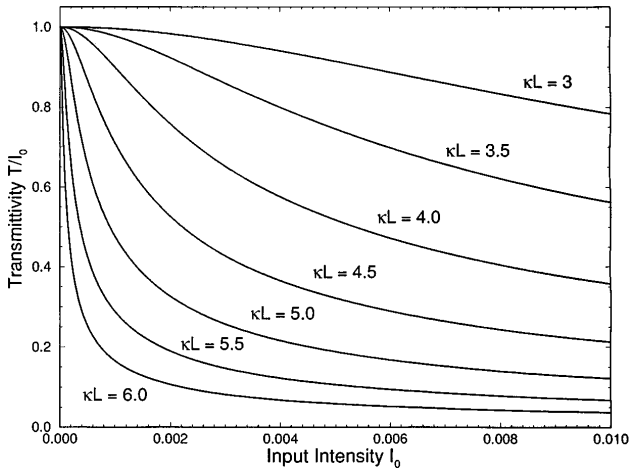

Fig. 6. Transmittivity of a nonlinear $\lambda/4$-shifted DFB structure in the case of zero detuning ($\Delta\beta L = 0$) for different values of the coupling strength κL. Even small variations in the input intensity ($\Delta I_0 \sim 0.2\%$) produce rapid changes in transmittivity ($\sim 90\%$) for moderate coupling strengths ($\kappa L = 6$).

to increase the input intensity to 0.2% of the critical intensity to decrease the device transparency from 100% to 10% and reach the off transmission state. Required switching intensity is directly related to the width of the central transmission peak. A structure with a stronger DFB coupling possesses a narrower peak and, consequently, allows a lower input to produce the above switching effect. One would naïvely suspect that for certain negative detuning values a reverse process of transmission increase (off-to-on switching) is also possible. This is true only in part, for a much more complicated behavior is observed in the case of finite detuning values.

B. Input–Output Characteristics

When Eqs. (44)–(47) are combined, it is possible to obtain complete input–output characteristics of a $\lambda/4$-shifted device for arbitrary values of the detuning parameter. Figure 7 shows these characteristics for a device with $\kappa L = 4$, for several detunings $\Delta\beta L$ in the range -0.6 to 0.6. It is evident from Fig. 7 that a true bistable behavior can be expected for negative detuning values as low as $\Delta\beta L \sim -0.3$ and for the extremely low input intensities $I_0 \sim 0.005$. This should be contrasted with the corresponding values for uniform DFB structures shown in Figs. 4 and 8. The plots in these figures are generated by use of Eqs. (23), (28), (30) and a coupling strength of $\kappa L = 4$. Achieving total transparency for the uniform structure tuned at a center of the stop band requires a normalized input intensity of approximately[10] $I_0 \sim 1$. This requirement can be lowered if one tunes near the stop-band edge, as shown in Fig. 8. Even in this case, intensities required for reaching the bistable operating region ($I_0 \sim 0.05$) are still an order of magnitude higher than those of $\lambda/4$-shifted structure for otherwise identical devices.

The effects of the reflection at the output of the device ($z = L/2$) are important if the cascading or the integration of the device is considered and are shown in Fig. 9a for the fixed reflectance phase ($\theta_R = \pi$) and $\Delta\beta L = -0.5$. As the end reflectivity is increased, more of the backpropagating light is coupled into the structure, resulting in a lowering of the upswitching threshold: the threshold of ~ 0.017 for the nonreflective case is lowered to ~ 0.011 if 30% reflectivity is introduced. Figure 9b shows the effects of the reflection phase on the input–output characteristics of the device for the case of 2% end reflectivity. Whereas a phase shift of π helps to lower the switching threshold, the $\pi/2$ shift has an opposite effect. It is of interest to mention that Fabry–Perot reflective conditions have been studied before in connection with the uniform nonlinear DFB structures.[30] However, such a device can be regarded as a hybrid Fabry–Perot/DFB rather than the DFB structure considered here.

C. Central Transmissive Peak Behavior

The switching behavior seen in Fig. 6 can be attributed intuitively to the notion that the central transmissive peak shifts as the intradevice field intensity is increased. Figure 7 implies that such a picture is valid only if the output intensity T is held fixed throughout the detuning region $\Delta\beta L$. Indeed, our method is actually designed by following this concept: we have prescribed the output intensity T first and then moved to find the corresponding output intensity I_0 for each value $\Delta\beta L$ within the

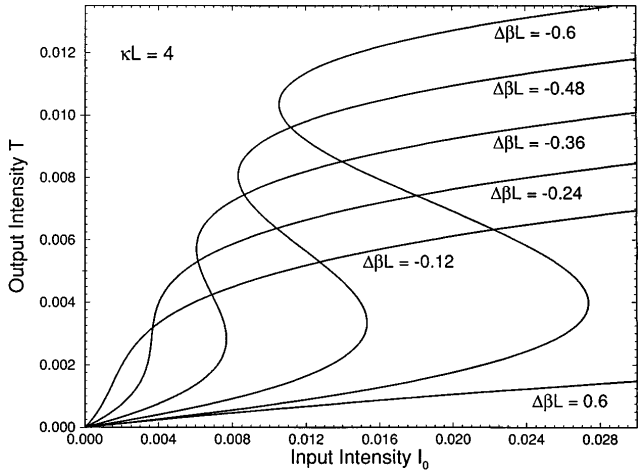

Fig. 7. Input–output characteristics of a nonlinear $\lambda/4$-shifted DFB device for $\kappa L = 4$. The detuning parameter $\Delta\beta L$ is varied between -0.6 and 0.6.

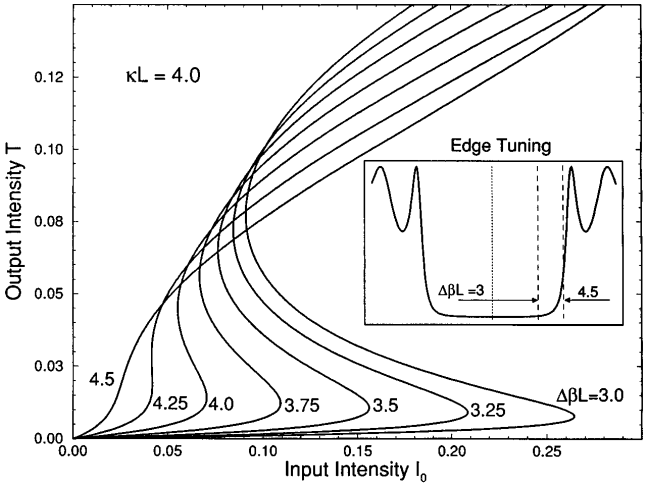

Fig. 8. Input–output characteristics of the uniform DFB device for $\kappa L = 4$ when the detuning parameter $\Delta\beta L$ is chosen close to the stop-band edge (inset).

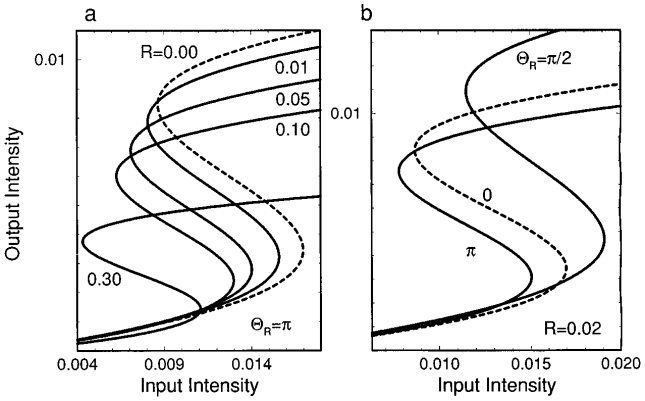

Fig. 9. Effects of the end reflection on the device performance. a, Input–output characteristics for fixed reflectance phase ($\theta_R = \pi$) and varying reflectivity R. b, Input–output characteristics for fixed reflectivity $R = 2\%$ and varying reflectance phase. The detuning parameter in both cases is set to $\Delta\beta L = -0.5$.

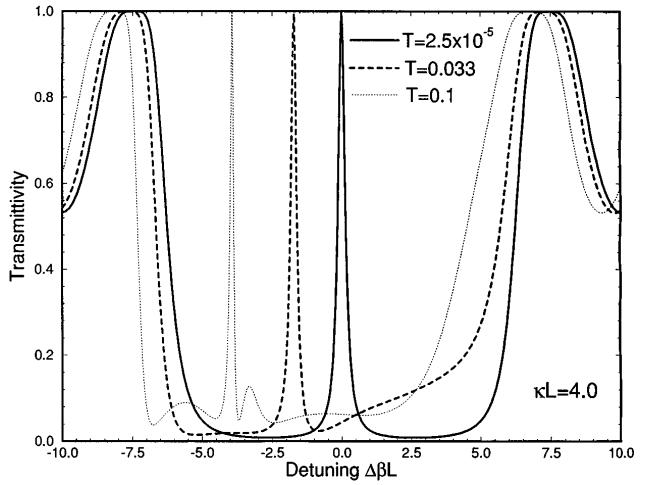

Fig. 10. Shifting behavior of the central transmissive peak for a $\lambda/4$-shifted DFB structure with $\kappa L = 4$. The normalized output intensity T is kept as the fixed parameter across the entire detuning range. The solid curve corresponds to the normalized output intensity of $T = 2.5 \times 10^{-5}$, the dashed curve corresponds to $T = 0.033$, and the dotted curve corresponds to $T = 0.1$.

tuning range. Figure 10 shows the transmittivity of the $\lambda/4$-shifted structure with $\kappa L = 4$, for three values of the output intensity: $T = 2.5 \times 10^{-5}$, 0.033, 0.1. The shifting of the center transmission peak can be recognized as an almost perfect tunable-filter behavior, justifying our initial expectations. Nevertheless, the plot in Fig. 10 can be considered both informative and misleading at the same time. In most cases of practical interest, one continuously changes the input I_0, not the output T, maintaining it as a fixed parameter throughout the frequency-tuning region. Consequently, the use of the transmittivity label in Fig. 10, where the output T is a fixed parameter while the input I_0 varies accordingly, can be questioned. For fixed input intensities, as implied by Fig. 7, the true transmittivity plots are quite different from those shown in Fig. 10. Figure 11 shows the change induced in the central transmission peak of the $\lambda/4$-shifted structure (characterized by $\kappa L = 4$) when the input intensity I_0 is the fixed parameter. The transmission efficiency is plotted for four values, $I_0 = 5 \times 10^{-5}$, 3.5×10^{-3}, 0.01, 0.015. It is clear from Fig. 11 that the reversal of the switching process described in Fig. 6 can be performed only if the bistable operation region, starting at $\Delta\beta L \sim -0.3$, is carefully avoided. Otherwise, a bistable switching will occur, for a given case of $\kappa L = 4$, at normalized input intensities as low as $I_0 \sim 0.01$.

D. Bistable Switching by Frequency Tuning

Figure 11 suggests the possibility for the use of the $\lambda/4$-shifted DFB structure as a new class of device in which bistable switching is controlled by frequency tuning while input intensity is maintained at a fixed, relatively low level. Figure 12 describes the operation of such a device in the case of a constant normalized input $I_0 = 0.01$ and a coupling parameter $\kappa L = 4$. By increasing the frequency of a tunable source one can make the device jump into high-transmission state $1'$ after it passes point 1 at $\Delta\beta L \sim -0.4$. Similarly, the low-transmission state $2'$ is achieved after the device passes point 2 at $\Delta\beta L \sim -0.6$ when moving in the opposite direction. This concept,

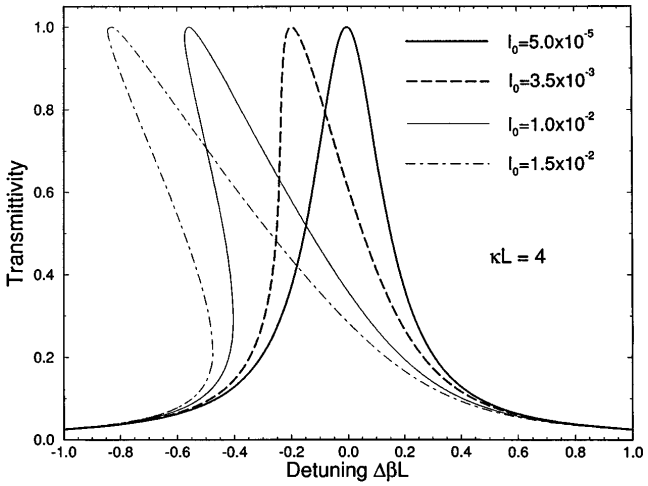

Fig. 11. Transmittivity of a $\lambda/4$-shifted DFB structure as a function of $\Delta\beta L$ when the normalized input intensity I_0 is kept fixed and the output T varies accordingly. The coupling strength of the structure is $\kappa L = 4$.

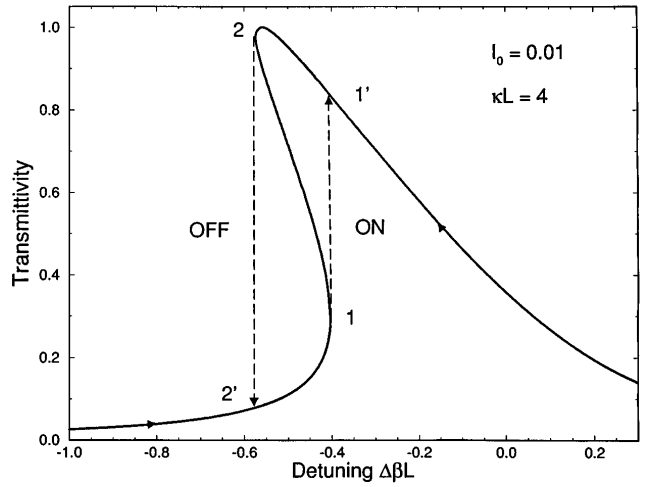

Fig. 12. Transmittivity of a $\lambda/4$-shifted DFB device as a function of $\Delta\beta L$ for $\kappa L = 4$ and normalized input intensity $I_0 = 0.01$. Wavelength tuning of the source with the fixed intensity I_0 leads to bistable switching, as shown by dashed lines.

recently proposed in connection with the Fabry–Perot semiconductor multilayered structure,[9] makes possible all-optical switching with a tunable, low-intensity optical source.

4. CONCLUSION

We have described the cw operating characteristics of nonlinear DFB phase-shifted structures by solving analytically the corresponding set of coupled-mode equations. The transmissive properties of a phase-shifted structure, commonly exploited in semiconductor laser design, have not been fully utilized in nonlinear switching applications. The advantages of the phase-shifted configuration presented in this paper include extremely low switching intensities (as much as 3 orders of magnitude lower compared with those for the uniform DFB structure) and the possibility of frequency-controlled all-optical switching at fixed, low input intensities. The model presented in this paper is applicable to a variety of guided-wave applications that satisfy the coupled-mode assumptions. A generalization to multiple phase-shifted DFB structures, similar to those used for reduction of spatial hole burning,[16] is straightforward from this model and is not limited specifically to the $\lambda/4$ phase shifts analyzed in this paper. We believe, however, that $\lambda/4$-shifted devices offer a simple and elegant approach to low-intensity, all-optical switching applications. Time-dependent analysis[13,31] applied to these types of structure is the next logical step in evaluating their use not only in cw but also in ultrafast applications.

APPENDIX A: CONSERVED QUANTITIES IN UNIFORM DFB STRUCTURES

Following the procedure outlined in Ref. 32, the magnitude and the phase of the counterpropagating field components are separated in the form

$$E_{\pm}(z) = |E_{\pm}(z)|\exp[i\phi_{\pm}(z)] = A_{\pm}(z)\exp[i\phi_{\pm}(z)]. \quad \text{(A1)}$$

Substituting Eq. (A1) into Eqs. (4), one can separate their real and imaginary parts to obtain the following four equations:

$$\frac{dA_+}{dz} = \kappa A_- \sin\psi, \quad \text{(A2)}$$

$$\frac{dA_-}{dz} = \kappa A_+ \sin\psi, \quad \text{(A3)}$$

$$A_+\frac{d\phi_+}{dz} = \kappa A_- \cos\psi + \gamma(|A_+|^2 + 2|A_-|^2)A_+, \quad \text{(A4)}$$

$$A_-\frac{d\phi_-}{dz} = \kappa A_+ \cos\psi + \gamma(|A_-|^2 + 2|A_+|^2)A_-. \quad \text{(A5)}$$

ψ is given by Eq. (8). Equations (A2) and (A3) lead directly to

$$\frac{1}{A_-}\frac{dA_+}{dz} = \frac{1}{A_+}\frac{dA_-}{dz},$$

which after the integration becomes the law of flux conservation:

$$A_+^2(z) - A_-^2(z) = \text{const.} = A_T^2. \quad \text{(A6)}$$

The straightforward way to prove that quantity Γ_i given by Eq. (7) is conserved within each region is to calculate its derivative $\partial\Gamma_i/\partial z$ and, using Eqs. (A2)–(A5), show that $\partial\Gamma_i/\partial z = 0$. A more elaborate proof, which assumes no prior knowledge of the form of Γ_i, is suggested in Ref. 27. This proof calls for the derivative of Eq. (8), which in combination with Eqs. (A2)–(A6) enables us to construct the relation

$$(-\cot\psi)\frac{\partial[\ln(A_+A_-)\cos\psi]}{\partial z} = 2\Delta\beta + 3\gamma(A_+^2 + A_-^2). \quad \text{(A7)}$$

Finally, the integration of Eq. (A7) yields the conserved quantity Γ_i in the form

$$\Gamma_i = A_+(z)A_-(z)\cos\psi_i(z) + [2\Delta\beta + 3\gamma A_-^2(z)]A_+^2(z)/(2\kappa). \quad \text{(A8)}$$

ACKNOWLEDGMENTS

This research is sponsored in part by the U.S. Army Research Office, the National Science Foundation, and the New York State Science and Technology Foundation.

REFERENCES

1. H. G. Winful and G. D. Cooperman, "Self-pulsing and chaos in distributed feedback bistable optical devices," Appl. Phys. Lett. **40,** 298–300 (1982).
2. W. Chen and D. L. Mills, "Optical response of nonlinear multilayer structures: bilayers and superlattices," Phys. Rev. B **36,** 6269–6278 (1987).
3. C. Martijn de Sterke and J. E. Sipe, "Extension and generalizations of an envelope-function approach for the electrodynamics of nonlinear periodic structures," Phys. Rev. A **39,** 5163–5178 (1989).
4. N. D. Sankey, D. F. Prelewitz, and T. G. Brown, "All-optical switching in a nonlinear periodic-waveguide structure," Appl. Phys. Lett. **60,** 1427–1429 (1992).
5. C. Martijn de Sterke and J. E. Sipe, "Switching dynamics of finite periodic nonlinear media: a numerical study," Phys. Rev. A **42,** 2858–2869 (1990).
6. H. G. Winful, "Pulse compression in optical fiber filters," Appl. Phys. Lett. **46,** 527–529 (1984).
7. H. G. Winful and G. I. Stegeman, "Applications of nonlinear periodic structures in guided wave optics," in *First International Conference on Integrated Optical Circuit Engineering*, S. Sriram and D. B. Ostrowsky, eds., Proc. Soc. Photo-Opt. Instrum. Eng. **517,** 214–218 (1984).
8. M. Okuda and K. Onaka, "Bistability of optical resonator with distributed Bragg-reflectors by using Kerr effect," Jpn. J. Appl. Phys. **16,** 769–773 (1977).
9. J. He and M. Cada, "Combined distributed feedback and Fabry–Perot structures with a phase matching layer for optical bistable devices," Appl. Phys. Lett. **61,** 2150–2152 (1992).
10. H. G. Winful, J. H. Marburger, and E. Garmire, "Theory of bistability in nonlinear distributed feedback structures," Appl. Phys. Lett. **35,** 379–381 (1979).
11. D. N. Christodoulides and R. I. Joseph, "Slow Bragg solitons in nonlinear periodic structures," Phys. Rev. Lett. **62,** 1746–1749 (1989).
12. C. Martijn de Sterke and J. E. Sipe, "Launching of gap solitons in nonuniform gratings," Opt. Lett. **18,** 269–271 (1993).
13. C. Martijn de Sterke, "Simulations of gap-soliton generation," Phys. Rev. A **45,** 2012–2018 (1992).

14. H. A. Haus, "Matching of distributed-feedback structures," Opt. Lett. **15,** 1134–1136 (1992).
15. H. A. Haus and C. V. Shank, "Antisymmetric taper of distributed feedback lasers," IEEE J. Quantum Electron. **QE-12,** 532–539 (1976).
16. G. P. Agrawal and A. H. Bobeck, "Modeling of distributed feedback semiconductor lasers with axially-varying parameters," IEEE J. Quantum Electron. **QE-24,** 2407–2414 (1988).
17. K. Utaka, S. Akiba, K. Sakai, and Y. Matsushima, "$\lambda/4$-shifted InGaAsP DFB lasers," IEEE J. Quantum Electron. **QE-22,** 1042–1051 (1987).
18. M. Yamada and K. Sakuda, "Analysis of almost-periodic distributed feedback slab waveguides via a fundamental matrix approach," Appl. Opt. **26,** 3474–3478 (1987).
19. G. P. Agrawal and S. Radic, "Phase-shifted fiber bragg gratings and their application for wavelength demultiplexing," IEEE Photon. Technol. Lett. **6,** 995–997 (1994).
20. H. W. H. Lee, R. S. Hughes, J. E. Davis, C. F. McConaghy, A. V. Hamza, and M. Balooch, "Feasibility of fullerene thin films for high-speed all-optical switching," in *Conference on Lasers and Electro-Optics*, Vol. 8 of 1994 OSA Technical Digest Series (Optical Society of America, Washington, D.C., 1994), p. 59.
21. W. E. Torruellas, D. Neher, R. Zanoni, G. I. Stegeman, I. Kajzar, and F. Leclerc, "Dispersion measurements of the third-order nonlinear susceptibility of polythiophene thin films," Chem. Phys. Lett. **175,** 11–16 (1990).
22. B. S. Kawasaki, K. O. Hill, D. C. Johnson, and Y. Fujii, "Narrow-band Bragg reflectors in optical fibers," Opt. Lett. **3,** 66–68 (1978).
23. K. O. Hill, B. Malo, F. Bilodeau, and D. C. Johnson, "Photosensitivity in optical fibers," Annu. Rev. Mater. Sci. **23,** 125–157 (1993).
24. J. Stone, "Photorefractivity in GeO_2-doped silica fibers," J. Appl. Phys. **62,** 4371–4374 (1987).
25. G. P. Agrawal, *Nonlinear Fiber Optics*, 2nd ed. (Academic, San Diego, Calif., 1995).
26. H. Kogelnik and C. V. Shank, "Coupled-wave theory of distributed feedback lasers," J. Appl. Phys. **43,** 2327–2335 (1972).
27. A. Yariv, "Coupled-mode theory for guided-wave optics," IEEE J. Quantum Electron. **QE-9,** 919–933 (1973).
28. H. G. Winful, "Optical bistability in periodic structures and in four-wave mixing processes," Ph.D. dissertation (University of Southern California, Los Angeles, Calif., 1980).
29. P. F. Byrd and M. D. Friedman, *Handbook of Elliptic Integrals for Engineers and Scientists* (Springer-Verlag, Berlin, 1971).
30. H. G. Winful, "Effect of end reflection on distributed-feedback bistable optical devices," IEEE J. Quantum Electron. **QE-17,** 164 (1981).
31. S. Radic and N. George, "Ultrafast pulse propagation in periodic optical media: a generalized finite-difference time-domain approach," Opt. Lett. **19,** 998–1000 (1994).
32. J. A. Armstrong, N. Bloembergen, J. Ducuing, and P. S. Pershan, "Interactions between light waves in a nonlinear dielectric," Phys. Rev. **127,** 1918–1939 (1962).